MOUNTAIN WAVES: MODELLING ASPECTS

Terry L. Clark
National Center for Atmopheric Research[1]
Boulder, Colorado 80307, USA

W.R. Peltier
Department of Physics, University of Toronto
Toronto, Ontario, Canada

1. Introduction

This paper emphasizes certain technical problems involved in the modelling of air flow over topography. Only those models which consider resolutions on the gravity wave scale will be discussed. These models are designed to explicitly model the dynamics of mountain wave drag and can be used as one basis for the parameterization of wave drag in larger scale models.

An important consideration in the design of such models is that of a proper representation of the nonlinear surface boundary condition. Miles and Huppert (1969) present analytical formulae showing the effect of a finite amplitude obstacle in two spatial dimensions. More recently this work has been extended to consider a wider range of conditions by Lilly and Klemp (1979). It has become well known that the finite height effect of the topography can have a first order effect on the predicted wave amplitude even prior to supercritical (wave breaking) conditions. By far the most popular approach of representing the nonlinear effects of the lower boundary condition has been to use a vertical coordinate transformation of the governing equations. Except for the pressure gradient terms, it is relatively easy to write a code that maintains the conservation characteristics allowed in a finite-difference Cartesian system. Certain aspects of such an approximate set of equations will be presented. The transformation approach eliminates the high frequency excitations associated with fitting the topography to a pattern of steps.

---

[1]The National Center for Atmospheric Research is funded by the National Science Foundation.

Finite element techniques provide an attractive alternative to the transformed models but this method is in itself complicated and has seldom been used in general small scale modelling of airflow over topography. An interesting approximate method of treating the nonlinear surface boundary condition was used by Mason and Sykes (1978) who represent the topography in a Cartesian system of equations as regions of arbitrarily high viscosity and density. The range of application of this method appears to be somewhat limited.

Some of the rationale for choosing between hydrostatic and non-hydrostatic filtered equation systems will also be presented. A particular implication for the design of a multi-domain or grid nested calculation will be described. Issues of accuracy and computational efficiency will be only briefly considered.

Two major issues in the modelling of small scale mountain air flow are initialization and the upper boundary condition. A general categorization of the type of initialization schemes employed is presented in Section 4. The upper boundary condition treatments will be outlined in Section 5.

Sections 6 and 7 present an outline of some of the modelling results that relate to the severe windstorm event. These sections emphasize nonlinear cases with supercritical Froude number flow in which wave breaking effects are believed to be of major importance. With the exception of a simulation by Clark and Farley (1984) the numerical simulation of severe windstorm events has been confined to two-spatial dimensions. It seems worthwhile to consider the effects of such an idealization on some of the important features of the simulated event. Comparisons will be presented between the two- and three-dimensional simulations from Clark and Farley's work.

An exhaustive, in-depth treatment of the physical and numerical considerations of modelling airflow over topography is not possible a single paper. As a result many aspects of the problem will be only briefly mentioned or altogether ignored. The role of moisture (Barcilon and Jusem, 1979 or Durran and Klemp, 1983) and the specification of lateral boundary conditions are two important areas not dealt with in this paper.

2. Coordinate Transformed Models

There have been a large number of hydrostatic models discussed in the literature. Only a few of these models have focused their efforts on a detailed understanding of the physics of forced gravity wave/mean flow

interaction or the problem of mountain drag. Some models base their vertical coordinate on potential temperature, θ, surfaces. A weakness of this approach is that the system of equations becomes indeterminate under conditions of neutral stability such as boundary layer flow or breaking waves. Deaven (1976) recognized such problems and designed a model based upon a combination of a θ and a sigma pressure coordinate transformation. His model was able to consider diabatic surface heating. Klemp and Lilly (1978) used a θ coordinate framework throughout the atmosphere to simulate the severe Boulder windstorm event of 11 January 1972 of Lilly and Zipser (1972). Diabatic surface heating was not treated and wave breaking problems were circumvented by employing a large eddy mixing coefficient in the region of wave breaking. Hoinka (1985) used the model of Mahrer and Pielke (1977) to study the same event. This hydrostatic model uses the sigma-z transformation

$$\eta = s(z-h)/(s-h) \tag{1}$$

where η is the transformed vertical coordinate. $s = s(x,y,t)$ is the model's upper lid and $h = h(x,y)$ is the height of the topography. The results of Hoinka (1985) suggest that this type of model is useful for general studies of the hydrostatic aspects of mountain drag.

The most obvious drawback of the hydrostatic model is that it does not treat problems correctly where the vertical momentum budget is important. Grid points where $w^2 \sim u^2$ is only one aspect of this problem. Linearly resonant lee waves, Scorer (1949), are totally filtered from these equations. Thus, the train of trapped lee waves moving downstream from a mountain source cannot be captured by such models. This weakness is probably of only minor significance to the mountain drag problem as these waves provide little vertical momentum transfer. The hydrostatic framework is not a particularly computationally efficient one once the horizontal grid size becomes relatively small. The Courant-Friedrichs-Lewy (CFL) condition is dominated either by Lamb waves or by the fastest moving external gravity wave. Thus, the time step must be kept relatively small since these modes travel at speeds near 300 m s^{-1}. There are some semi-implicit treatments which allow for mixed time steps. On the other hand, non-hydrostatic models are typically limited by the CFL criteria determined by the fastest moving internal gravity waves. These move at $\sim$30 m s^{-1}. Thus, the non-hydrostatic models can be much more efficient for smaller scale problems in spite of the added overhead required by the solution of a diagnostic elliptic equation. Cotton (personal

communication) estimates that the non-hydrostatic code is always more efficient for grid sizes $\leq$ 20 km. There is one further reason for considering the non-hydrostatic model which is associated with multi-domain or grid nesting. This point will be discussed later. The remainder of this section will consider technical aspects of only the non-hydrostatic models.

The two common types of non-hydrostatic model are the elastic and the anelastic codes. The elastic codes consider sound waves semi-implicitly as in Tapp and White (1976) and Carpenter (1979) using the techniques of Kwizak and Robert (1971). A diagnostic Helmholtz equation must be solved each time step in this case. Tripoli and Cotton (1982), and Durran and Klemp (1983) use the time splitting techniques of Marchuk (1974). The anelastic models such as that of Clark (1977), and Clark and Farley (1984) filter the sound waves according to Batchelor (1953), Dutton and Fichtl (1969) and Ogura and Phillips (1962). Both methods appear to have about the same level of efficiency since the small time step in the elastic time splitting codes consumes about the equivalent of the pressure solution. To date there is no evidence indicating that the sound waves are important for typical meteorological problems. There is some evidence indicating problems with the time splitting elastic code for cases of extreme topographical gradients. Cotton (personal communication) is currently converting to an anelastic framework because of problems he encountered in some recent studies. The inconsistent definition of divergence between the two time scales may be associated with this problem.

Conservation of momentum and energy have been considered to be of significant importance in meteorological modelling. This stems from computational and physical reasoning. It should also be recognized that conservation is not a necessary condition for the order of accuracy. For example, fourth order finite difference models do not conserve energy. Nevertheless, it seems worthwhile to outline some model design considerations which optimize conservation in a transformed coordinate model. Two sigma-z type transformations will be used for purposes of demonstration. Similar analysis should apply to other sigma-z choices.

The two coordinate transformations under consideration here transform from the usual (x,y,z) orthogonal Cartesian system onto the non-orthogonal $(\bar{x},\bar{y},\bar{z})$ system. These transformations are $\bar{x}=x$, $\bar{y}=y$, and

$$\bar{z} = H(z-h)/(H-h) \qquad (2)$$

as in Gal-Chen and Somerville (1975) and Clark (1977) or

$$\bar{z} = h - z \tag{3}$$

as in Carpenter (1979). H is the height of the model lid and h=h(x,y) is the terrain height. Both of these transformations map an irregular lower boundary onto a regular grid. The deformation of the Cartesian grid is maximum near the surface in (2) whereas it is uniform with height in (3). Following Gal-Chen and Somerville (1975) the following tensor notations will be used.

$$G^{13} = \frac{\partial \bar{z}}{\partial x} \qquad G^{23} = \frac{\partial \bar{z}}{\partial y} \qquad \sqrt{G} = \frac{dz}{d\bar{z}} \tag{4}$$

As shown in Clark (1977) the momentum equations can be transformed and cast into numerically approximate forms as

$$\delta_t \bar{\rho}^x u + \delta_x\left(\overline{\bar{\rho}^x u}^x \bar{u}^x\right) + \delta_y\left(\overline{\bar{\rho}^y v}^x \bar{u}^y\right) + \delta_z\left(\overline{\bar{\rho}^z \omega}^x \bar{u}^z\right) = -\delta_x\left(\sqrt{G}\, P\right) - \delta_z\left(\sqrt{G}\, G^{13} \bar{P}^{xz}\right) \tag{5}$$

$$\delta_t \bar{\rho}^y v + \delta_x\left(\overline{\bar{\rho}^x u}^y \bar{v}^x\right) + \delta_y\left(\overline{\bar{\rho}^y v}^y \bar{v}^y\right) + \delta_z\left(\overline{\bar{\rho}^z \omega}^y \bar{v}^z\right) = -\delta_y\left(\sqrt{G}\, P\right) - \delta_z\left(\sqrt{G}\, G^{23} \bar{P}^{yz}\right) \tag{6}$$

$$\delta_t \bar{\rho}^z w + \delta_x\left(\overline{\bar{\rho}^x u}^z \bar{w}^x\right) + \delta_y\left(\overline{\bar{\rho}^y v}^z \bar{w}^y\right) + \delta_z\left(\overline{\bar{\rho}^z \omega}^z \bar{w}^z\right) = -\delta_z P + g\bar{\rho}^z \overline{\left(\theta'/\bar{\theta}\right)}^z \tag{7}$$

$$\delta_x\left(\bar{\rho}^x u\right) + \delta_y\left(\bar{\rho}^y v\right) + \delta_z\left(\bar{\rho}^z \omega\right) = 0 \tag{8}$$

where $\delta_\eta \phi = \left(\phi(\eta+\Delta\eta/2) - \phi(\eta-\Delta\eta/2)\right)/\Delta\eta$ and $\bar{\phi}^\eta = \left(\phi(\eta+\Delta\eta/2) + \phi(\eta-\Delta\eta/2)\right)/2$ are Schuman (1962) type operators. These equations assume a staggered grid framework. Coriolis and subgrid scale mixing terms are not shown in (5) - (7) but are typically included in the codes. The conservation equations for θ etc. are also not shown as they do not directly relate to the discussion at hand. Now (5) - (7) are the original Cartesian momentum equations and as such will conserve all three components of momentum irrespective of the topography. If we had gone straight to the tendency equations for $\dot{\omega} = (d\bar{z}/dt)$ as in Gal-Chen and Somerville (1975) or Carpenter (1979) then Christofel terms would be evident. They are not yet evident in (5) - (7) because they occur as a result of the combination of these three equations plus the relationship between ω and u,v,w, and h when forming the $\dot{\omega}$ equation. Applying the

numerical approximations at the last stage ($\dot{\omega}$ equation) can result in lack of conservation of vertical momentum as well as energy unless an extensive stencil is employed.

The conservation principles of Arakawa (1966) have been used in the derivation of (5) - (8) so that the nonlinear advection terms also conserve kinetic energy for arbitrary topography except for the usual temporal truncation errors. A momentum and energy conserving ω tendency equation can be derived by combining (5) - (7) through a definition of ω such as

$$\sqrt{G}\,\overline{\rho}^{z}\omega = \overline{\rho}^{z}w + \sqrt{G}\,G^{13}\,\overline{\overline{\rho}^{x}u}^{z} + \sqrt{G}\,G^{23}\,\overline{\overline{\rho}^{y}v}^{z} \quad . \tag{9}$$

Such a procedure will result in a horribly complicated but conservative numerical form for the Christofel terms. The models of Gal-Chen and Sommerville (1975) and Carpenter (1979) did not follow this procedure and as a result do not conserve momentum or kinetic energy as prescribed by the equations of motion. The models of Tripoli and Cotton (1982), Durran and Klemp (1983) followed the conservative formulation of Clark (1977) although other aspects of their models differ.

In order to solve equations (5) - (9) the tendencies are eliminated to form a diagnostic pressure equation. The semi-implicit elastic models combine (5)-(7) and (8) plus a pressure tendency equation to form a diagnostic divergence equation. This results in a rather complicated elliptic equation where some special techniques are useful. This equation can be solved using block iteration, successive over relaxation or multi-grid techniques. The pressure equation in Clark (1977) results in a 25 point stencil by treating all terms involving h explicitly. Carpenter (1979) retained a 15 point stensil by treating all terms involving h explicitly.This is essentially equivalent to a single block iteration in Clark's scheme. Serious problems have occurred in Clark's model in cases of very steep slopes (>40°) using the block iteration scheme. Recently, Clark (1986) introduced an under relaxation approach to his model. After each block iteration, except the last, only a fraction of the diagnosed pressure solution correction is accepted. This under relaxation compensates for any over predictions caused by retaining only half the pressure gradient terms in the direct (or block iteration) portion of the pressure algorithm. As a result of this procedure, slopes ~40° could be modelled using two block iterations and slopes > 52°

could be modelled using three block iterations without having to reduce the time step. This difficulty in the anelastic system may relate to the problems discussed earlier in the elastic system of Tripoli and Cotton. Furthermore, it would be interesting to see if there is a similar topographic slope limitation to the Carpenter (1979) model where again only half of the appropriate pressure gradient term is treated in his diagnostic equation.

There does not appear to be any currently used scheme that allows for precise conservation of kinetic energy in these non-hydrostatic models because of the pressure gradient terms. Clark (1986) shows that the truncation error production of kinetic energy by the pressure gradient terms in two-dimensions, PTRE, using (2) is

$$\text{PTRE} = \frac{\Delta z}{4}\,\delta_z\left[Z(\delta_z \overline{h_x u}^{x})\;\delta_z P\right] + \frac{\Delta x^2}{4}\,\delta_x\left[h_x u Z\;\overline{\delta_{xz} P}^{z}\right] \qquad (10)$$

where $Z = (\bar{z}/H-1)$ and ρ_0 = constant. The error is typically maximum near the surface and decreases to zero at the domain top ($\bar{z}=H$). This decrease is usually much faster than linear because of the associated field structure having maximum gradients near the surface. The error structure using (3) in Clark's model is obtained by putting $Z = -1$ in (10). Thus, a linear decrease with height of this conservation error associated with Z is lost when using the transformation which has uniform deformation of the Cartesian coordinates with height. Reasonable choices of resolution with respect to the topography typically result in (10) being negligible as shown in Clark (1977) for the case of (2) and these results should also apply to the case of (3). One should be careful to monitor (10) or its equivalent form in three-dimensions when using significant slopes in the orography. It was also shown in Clark (1977) that a significant reduction in (10) was accomplished by subtracting the horizontally uniform portion of buoyancy from (7). Such subtractions reduce the magnitude of P.

3. Grid Nesting Considerations

The necessity for multi-domain (or grid nesting) simulations may also influence ones decision in choosing between an hydrostatic or anelastic code. For example, increased resolution may be desirable in the boundary layer or in a convectively unstable wave breaking region. Following concepts of the multi-grid literature it is desirable to have the finer mesh domains consistent with the coarse mesh domain model over

their equivalent computational domain. This consistency means that if one appropriately averages the fine mesh equations onto the coarse mesh resolution, then the averaged fine mesh and coarse mesh equations are identical. Under such conditions the substitution of fine mesh solutions into the coarse mesh solutions becomes redundant. Consistent multi-domain codes should avoid many of the numerical problems familiar to the meteorological community in the interactive nesting of finite difference mesoscale models. The ability to write a consistent multi-domain code depends upon the form of equations. Hyperbolic equations are initial value in nature where the solutions follow characteristics. Hyperbolic equations do not seem to allow for the writing of a consistent multi-domain code because of their local nature. The parabolic terms are also local in nature. The shallow water equations are hyperbolic and in general the hydrostatic models tend to be hyperbolic in the horizontal. The hydrostatic model of Kurihara et al. (1979) provided a consistent matching of the continuity equation by using a consistent (or reversable) set of averaging and interpolation formulae but this model cannot have a consistent treatment of the momentum equations. The anelastic model of Clark and Farley (1984) had a similar level of consistency. More recently Clark (1986) has shown that the anelastic model has a sufficient degree of ellipticity through the diagnostic pressure equation that a consistent treatment of the momentum equations is also possible with a negligible increase in computational cost. This version of the code is currently undergoing testing. It appears that the hydrostatic model equations have applied too much filtering to the original equations to allow for such consistent multi-domain simulations. Although possible in principle in the elastic codes this procedure appears to be more complicated even when the full pressure gradient is considered in the diagnostic Helmholtz equations. Thus, from a multi-domain simulation viewpoint the existing anelastic codes appear to have an advantage at the present time.

4. Initialization or Start-Up Procedures

This is one of the major problem areas for small scale limited area modelling of airflow over mountainous terrain. There is a real need for much more systematic work on procedures to initialize hydrostatic and particularly non-hydrostatic models on the small scale. The ad hoc procedures in use can be categorized into three general areas. A subcritical Froude number initialization scheme is one that approaches the final

value of Fr^{-1} (=Nh/U) starting from subcritical values. Examples of subcritical Fr initialization are the "diastrophism" of Deaven (1976) where the mountain is slowly built up with time. A variation of this approach being tested on Clark's model is surface boundary relaxation where the flow is initially allowed to flow through the mountains. Slowly with time the boundary condition is relaxed to $\omega=0$ at $\bar{z}=0$. A supercritical Fr initialization is one that approaches the final value of Fr starting from supercritical values. Building the mean flow with time as in Peltier and Clark (1979, 1983) or Durran and Klemp (1983) is an example of such an initialization procedure. In both of these time dependent initialization schemes, the results are sensitive to the choice of initialization time scale. Intuitively, supercritical initialization should be by far the most sensitive because one is starting with blocked flow until Fr>1 is achieved. Thus, the very purpose of a smooth start-up to avoid high frequency solution effects (e.g., see Fig. 3 of Peltier and Clark, 1983) by choosing a long time scale might be offset by the too long duration of supercritical conditions if too large a time scale is chosen. There does appear to be a fair degree of sensitivity of the early time (first few hours) results depending upon the choice of this time scale. Fig. 12 from Durran and Klemp (1983) shows a comparison between the 2-D mountain drag solutions and those of Peltier and Clark (1979). There appears to be an underdamped character to both of these drag curves for these two supercritical Fr initialization schemes. Neither of these experiments were integrated long enough to reach a "steady-state" wave drag as occurred in Clark and Farley (1984). This required about 140 min in their case but using a stationary Fr number initialization scheme.

A stationary Fr number initialization scheme is one in which the initial flow assumes the flow field far upstream of the mountain that equals the final desired Fr forcing for the problem under consideration. Examples of stationary initialization are those of Carpenter (1979), Clark and Peltier (1984), and Clark and Farley (1984). Carpenter used a combination of Ekman layer equations, interpolation from a large-scale model and Richardson's equation. One problem noted with this approach was that of an imposed net mass inflow through the lateral and upper boundary. Clark developed a stream function initialization which can be applied only in cases where the mountain has a two dimensional structure such as a uniform ridge. The vorticity of the flow is assumed equal to the far upstream value which allows the formulation of a Poisson equation

for the stream function of the flow in the plane normal to the mountain. This is not a potential flow initialization because of the allowance for vorticity and more importantly because the isentropes are not initialized such that $\theta = \theta(x,z)$. Instead $\theta = \theta(z)$ which means that the initial horizontal gradients of buoyancy are zero resulting in the first time derivative of vorticity being zero. This procedure appears to work reasonably well but again no detailed analysis has been performed. Fig. 11 from Clark and Farley (1984) shows some drag plots versus time using this scheme where the response shows an underdamped character. There is as much early time difference between the drag plots from Clark and Farley and Peltier and Clark (1979) as there was between Peltier and Clark and Durran and Klemp for the Boulder windstorm simulation.

There is a real need to understand the existing schemes and develop new schemes for initialization. Both the early time and so-called steady state solutions, and the time required to relax onto steady state, need to be accessed. Presently it is impossible to differentiate between effects of resolution, other model dependent assumptions, and initialization for certain aspects of the simulations of severe mountain drag cases. From a parameterization viewpoint, initialization could be an important consideration because the large scale forcing is continually changing on a supposed long time scale. Whether the mean flow is accelerating or decelerating into a severe event may require some consideration of the type of initialization employed. It may be advisable to consider coupling the small scale models to much more extended areal extent models so that far upstream influences as noted by Pierrehumbert and Wyman (1985) can be considered, i.e. the assumption of steady forcing could be addressed on a range of scales. Nesting as discussed in Section 3 might be appropriate for such studies.

5. Radiation Boundary Condition

A major problem in forced gravity wave simulations is that the models have a limited vertical extent. The atmosphere allows wave energy to escape to very high levels far exceeding those of the tropopause. Thus, is is necessary to devise methods where the upper lid of the model appears as $z = +\infty$ to the lower level waves. The oldest and most common approach has been to use an absorber region where vertically propagating waves are damped either by Rayleigh friction or by a large eddy mixing coefficient. Klemp and Lilly (1978) use a horizontal mixing coefficient

and they provide an analysis of the upper level reflection characteristics. Clark and Peltier (1977, 1984) and Peltier and Clark (1979) used an eddy mixing coefficient which was active also in the vertical direction. Clark (1977), Clark and Farley (1984), and Durran and Klemp (1983) used a Rayleigh friction absorber. It has been shown that an absorber must be at least one vertical wave length deep to be effective, where the vertical wave length is usually taken as that corresponding to the hydrostatic wavelength, 2 U/N. The advantages of the absorber approach is that it is easy to implement, does not invoke a linearization assumption, and works as well for transient problems as for steady state problems. The major disadvantage is that it is computationally expensive, particularly for a non-nested simulation.

Another approach which has certain attractions is based upon the use of a linearized time dependent wave equation. Beland and Warn (1975) employed this approach in their study of horizontally propagating Rossby waves but also considered extension of the method to the case of vertically propagating gravity waves. In their system of equations, which is similar to that for vertically propagating internal waves, they discussed both the steady state and transient problems. The time dependent problem requires the retention of a history term which adds considerable computational cost to the boundary condition. Furthermore, the inverse Laplace transform can only be obtained by numerical methods except, as in their case, for very simplified environments. They did not test their steady state condition in their simulations. Klemp and Durran (1983) applied a slightly different radiation condition than Beland and Warn's steady state equations where pressure and vertical velocity are related at the model top. The form of Klemp and Durran equations and a comparison with those of Beland and Warn suggest that this particular form of the normal mode boundary condition should work well only for steady state problems. Nevertheless, this type of boundary condition is attractive due to its computational efficiency for many of the mountain drag problems of interest to the community. The influences of transients which occur in three-dimensional simulations such as Clark and Farley (1984) and which occur in the transient initialization phase have yet to be established.

Another problem associated with all of the above radiation treatments is an instability resulting from physical approximations made when invoking this radiation condition. The radiation condition assumes that all the wave energy is propagating vertically and that the

disturbance above some interface in no way interacts with those below. This is an approximation. Clark and Peltier (unpublished manuscript) found that their long term wave drag solutions for some subcritical flows continued to slowly grow with time. The reason for such behaviour, at that time, was not understood. More recently, Klemp and Durran (1983) shed light on the problem by producing similar results and attributing them to the radiation condition itself. Their Fig. 7 shows quite clearly the sensitivity of the results to the location of the absorber. These results support Klemp and Durran's interpretation. Sensitivity experiments suggest that this instability is considerably weakened by raising the level of the absorber well beyond one vertical wavelength. This presents an interesting dilemma for model design in certain experiments. How high should one really place the model lid particularly for subcritical flows? If the lid is placed "high enough" then does it really matter whether one uses a local radiation condition or an absorber? For many of these problems it is much easier to design a computationally stable, efficient, and generally applicable experiment using multi-domain methods. The upper boundary condition problem is easier to deal with in supercritical flows because of the large amount of wave energy that is reflected from the wave breaking region. There is, though, still the amount of wave energy associated with the critical stream line steepening propagating beyond the wave breaking region as discussed by Peltier and Clark (1983).

6. Comparison of Two- and Three-dimensional Severe Storm Simulations

Two-dimensional numerical simulations have been extensively used to study the dynamics of severe downslope windstorms. Most of the studies have concentrated on the observed case of 11 Jan 1972. Fig. 1 shows interpretations of θ and u based upon aircraft observations by Lilly and Zipser (1972) of this Boulder windstorm event.

An early explanation for the severity of this type of windstorm was based upon linear theory concepts. Klemp and Lilly (1975) hypothesized that the thermal stability variations associated with the tropopause caused partial reflection of vertically propagating wave energy. They also considered the effect of the lower level inversion. Using a three layer model of the atmosphere where the stability and mean flow were idealized, they suggested a maximum response would be obtained when the tropopause was $\lambda_z/2$ above the surface for their symmetrical mountain case. This "tuned" height corresponded to a case of constructive partial

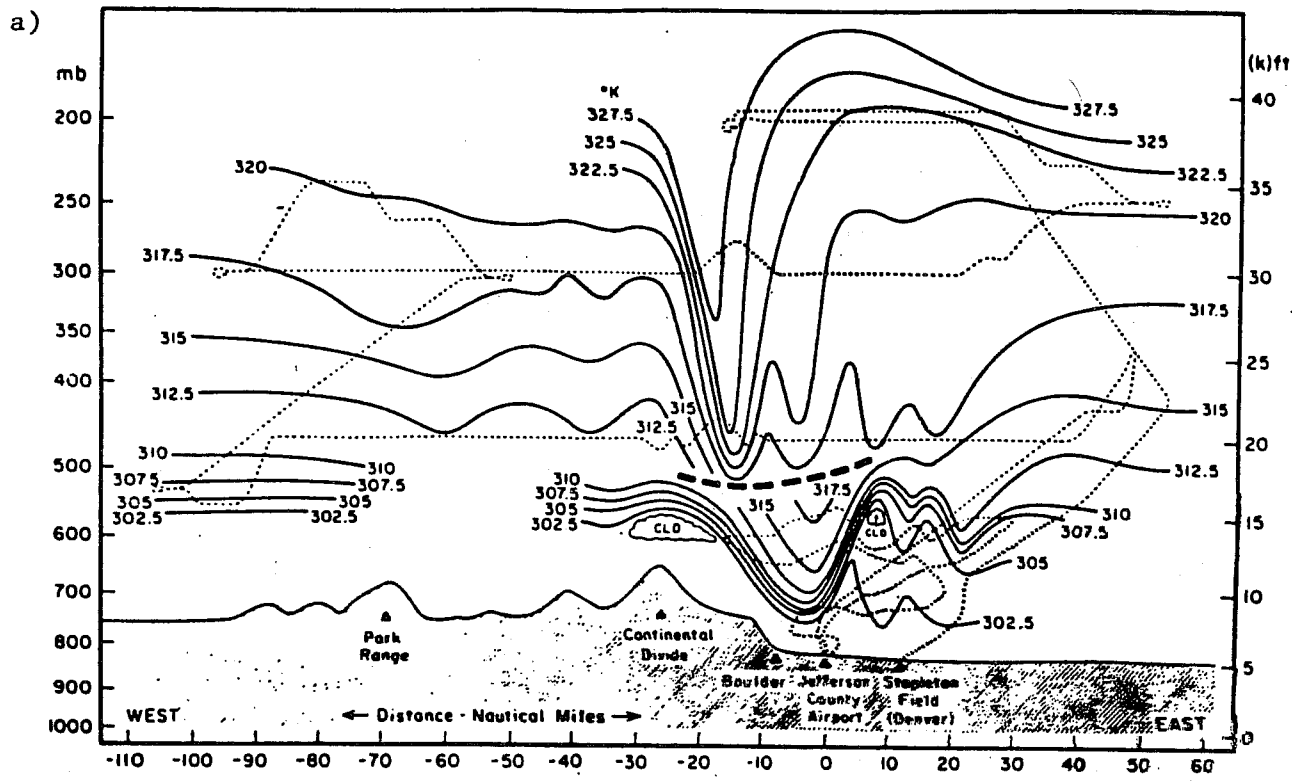

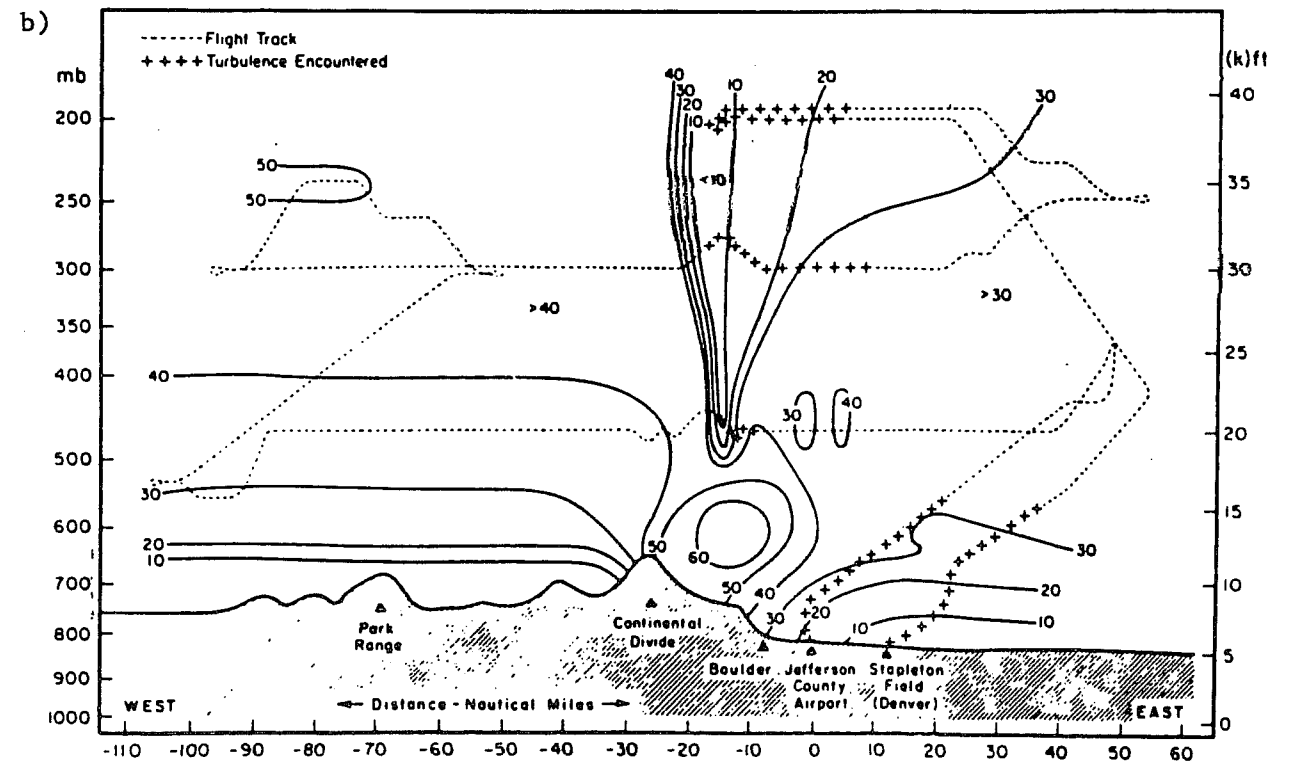

Fig. 1 a) Isentrope field for the 11 January 1972 severe wind storm in Boulder (after Lilly and Zipser, 1972).

b) Horizontal velocity field for the 11 January 1972 severe wind storm in Boulder (after Lilly and Zipser, 1972).

reflection. Klemp and Lilly (1978) introduced a much more realistic environment for the 11 January 1972 case and obtained a severe downslope event with their hydrostatic isentropic model. They interpreted their results using the same linear theory concept.

A discriminating experiment to test this linear theory hypothesis was designed by Peltier and Clark (1979). These authors suggested that the mechanism of enhanced wave drag was not due to partial reflection associated with the linear response of the atmosphere but was due to the partial reflection of wave energy associated with the non-linear wave breaking region. The height above the surface, for symmetrical mountain forcing, of maximum stream line steepening was shown to be 3/4 λ_z which differs from the earlier postulated $\lambda_z/2$ level. Thus, both the mechanism and, as a result, the height of occurrence were being questioned. The discriminating experiment designed was to simply run two experiments with different stratospheric wind speeds. The observed case of ~20 m/s stratospheric winds allowed for wave breaking whereas the ~35 m/s did not allow for wave breaking at the first level of maximum stream line steepening. The transmission/reflection coefficient characteristics of both atmospheres should be very similar so that if the linear theory interpretation were correct then both experiments should give similar severe responses. Peltier and Clark found that only the wave breaking case gave a severe response whereas the case with higher speed stratospheric winds gave a dramatically weaker response. This experiment cast considerable doubt upon the linear theory mechanism. More recently Hoinka (1985) repeated this experiment where the stratospheric winds were more gradually modified. His experiments showed a dramatic reduction in surface wave drag between the 30 m/s and 40 m/s stratospheric wind speed cases. There was approximately a factor of 3 reduction in drag intensity between these two states. Thus, these experiments support the concept of a bifurcation in solutions occurring which is due to the attainment of a critical level of steepening of the streamlines overhead of the mountain.

The wave breaking hypothesis is also subject to a discriminating experiment. Since this hypothesis does not rely at all upon vertical gradients of the Scorer parameter, it should also occur for cases where both the wind speed and static thermal stability are uniform with height. The nonlinear wave breaking hypothesis should show a bifurcation in the solutions between a subcritically Fr forced case and a supercritically Fr

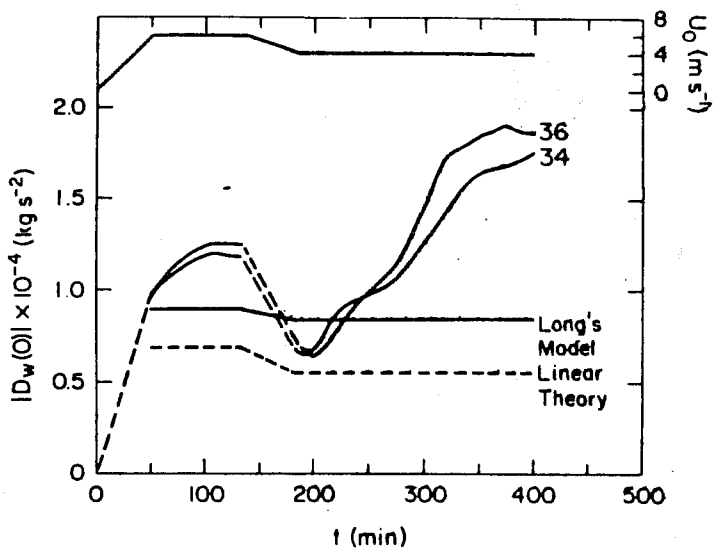

Fig. 2 Surface wave drag versus time. $U_0(t)$ shown in top portion where a bell shaped mountain with h = 400 m and half-width a = 3 km. Steady portions of U correspond to 5 m s^{-1}(Fr^{-1} = .79 subcritical) and 4 m s^{-1}(Fr^{-1} = .99, supercritical) (after Peltier and Clark, 1983).

forced case. Peltier and Clark (1983) show results for such an experiment. They performed a backoff experiment where a subcritical Fr flow was initialized using a supercritical Fr initialization scheme. After the maximum wave drag values were attained the flow speed was reduced to produce a supercritically forced state. The result was that the wave drag values linearly increased with time until they reached values ~ 2 times Long's values would predict where the nonlinear lower boundary condition is considered. Thus, the nonlinear wave breaking response hypothesis was supported. Researchers might consider further refinements of this type of experiment using different initialization procedures. One strong advantage of the Peltier-Clark backoff experiment is that it allows inspection of the Reynolds stress profiles as a function of time. Fig. 2 shows the wave drag, $|D_{w(0)}|$, versus time for this experiment whereas Fig. 3 shows the time history of the Reynolds stress profiles at, a) 20 min intervals for a subcritical case and b) at late time for the supercritical state of the backoff experiment. The Reynolds stress plots for the supercritical case show the stress at first increasing with time and finally reducing towards the expected constant with height values as predicted by Eliassen and Palm (1960) for the Longs model. Fig 3b shows a very different response for the supercritical flow. The stress is linearly increasing with time in the cavity between the ground and z = 3/4 λ_z. Above this level the stress assumes that value obtained from Long's model for the critical Fr^{-1} = .86 case for this problem. This idealized case suggests that a parameterization of wave drag for a

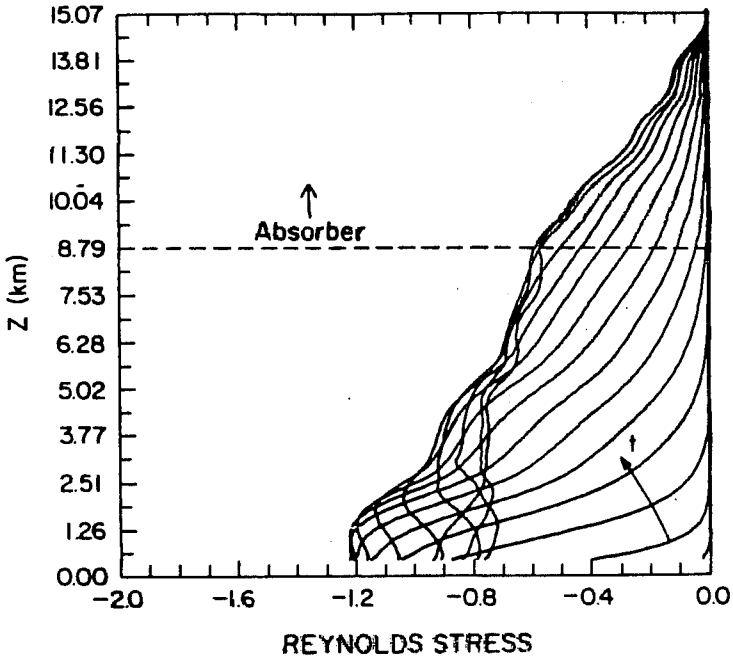

Fig. 3
a) Reynolds stress profiles at 20 min intervals for the case of U_0 = 5 m s^{-1}. A 200 Δt = 4.73 τ_N start up period was used building the flow from rest (after Peltier and Clark, 1983).

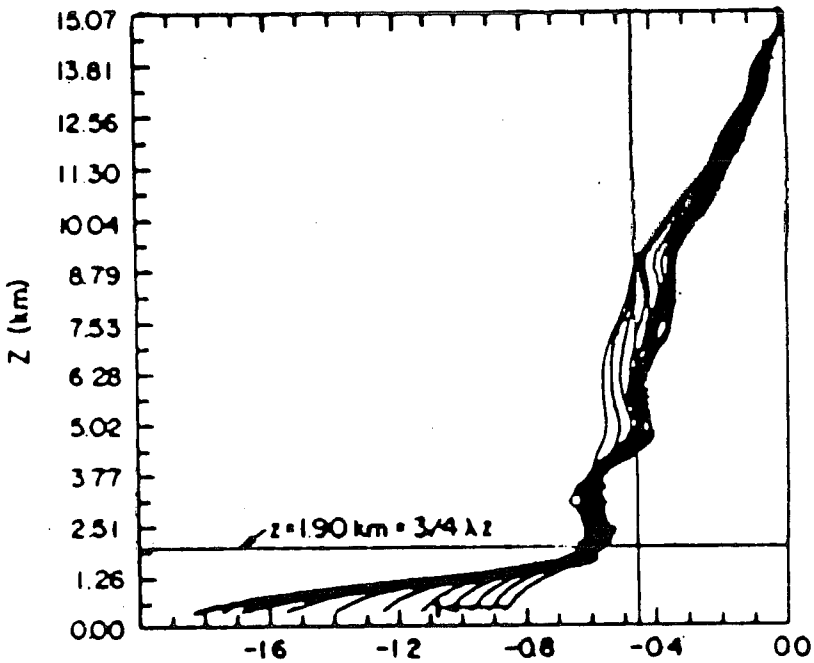

b) Reynolds stress from exp 36 (see Fig. 2) starting at t = 230 min withprofiles drawn every 10 min (after Peltier and Clark, 1983).

supercritically forced flow should equally deposit momentum throughout the cavity which has been established between the ground and the wave breaking region. Actual cases of severe mountain drag are typically complicated by variations in stability, moisture, and tropospheric jets. The results from Clark and Farley (1984) will be used to address the effects of the first and last of these complicatons. To date this paper represents the only detailed three-dimensional simulation of a severe windstorm event.

Clark and Farley (1984) present both two- and three-dimensional simulations of the 11 January 1972 Boulder windstorm. Clark (1987) also presents further analysis of the three-dimensional simulation where a turbulent kinetic energy budget analysis is presented. The mountain forcing in the three-dimensional experiment was taken as a two-dimensional ridge so that, except for the turbulence modelling in the wave breaking region, the three- and two-dimensional simulations are physically equivalent. Fig. 4 presents a comparison between the two- and three-dimensional Reynolds stresses obtained in these experiments.

Fig. 4(a) shows three time levels of the Reynolds stress for the two-dimensional experiments and (b) shows seven time levels for the three-dimensional experiments. The solid bars at z=0 denote the range of surface wave drag. The stress plots are still rather transient in nature in both cases. A rough eyeball fit to the curves suggests a nearly constant average rate of negative momentum deposition between the mountain top (h_0 level) and the tropopause (trop) level with a lesser amount of positive momentum deposition between the ground and the mountain top. The tropopause level corresponds with the upper levels of the wave breaking or convectively unstable region of the calculations. In both simulations a considerable amount of momentum is transmitted through the tropopause implying a slowing down of the stratospheric winds in the lee of the mountains.

The comparison between the two- and three-dimensional simulated Reynolds stresses in Fig. 4 shows that they are in many respects quite similar. A comparison of the field structures of the wind component directed normal to the mountain (or ridge in three-dimensions) and fields will indicate the degree to which the two-dimensional simulations might be expected to capture the basic dynamics for this particular severe event as well as other cases. These plots can also be compared to the observations shown in Fig. 1. Figs. 5 and 6 show the u and θ field comparisons between the two- and three-dimensional simulations. The plots for the three-dimensional simulations were obtained by taking a cross-stream average. The model was assumed cyclic and contained only 10 grid points in this direction. The basic purpose of including cross-stream points was to allow the fluid flow to become three-dimensional in character where vortex twisting and stretching would become active. Clearly, there is a need for further three-dimensional simulations of this type where increased cross-stream domain and resolution are

considered. Also, effects of the three dimensional character of the topography need to be considered. Except in the highly nonlinear convectively unstable or wave breaking region, the two simulations are quite similar. A wind reversal and commensurate overturning region are present at about the 8 km height overhead of the mountain in these simulations. These simulations as well as those of the previously cited authors compare quite favorably with the observations. Whether or not there was a wind reversal in the actual observations is not clear (Lilly, 1978). The wind reversal appears to be somewhat over emphasized by the two-dimensional models. This can be seen more clearly by comparing Fig. 1 of Clark (1987) with the present Fig. 5b for the same basic model. It may turn out that increased resolution for the three-dimensional model may reduce such reversal effects even further. Nevertheless, the two-dimensional models appear to perform quite faithfully for these idealized cases.

Lilly (1978) analyzed the aircraft data for the 11 January 72 Boulder windstorm. He estimated the wave drag to be in the range of .7 to 1.6×10^6 Kg/s^2. The numerical simulations predict values ranging from about 1.4×10^6 for the moist calculations of Durran ad Klemp (1983) and about 1.6×10^6 for the dry calculations of Durran and Klemp and Peltier and Clark (1979). Clark and Farley obtained 3.0×10^6 for their two-dimensional calculations and 2.5×10^6 Kg/s^2 for their three-dimensional case. All of these estimates are surprisingly close in spite of the weaknesses of the models in properly representing or resolving the turbulence. It is not surprising that slight differences in the models produce estimates differing by a factor of 2. The upstream boundary conditions are probably much steadier in the Clark and Farley cases because of their increased horizontal domain of 240 km and this may have influenced their increased estimates. Hoinka (1985) obtained $\sim 2.0 \times 10^6$ Kg/s^2 using a similar domain in an hydrostatic model.

7. Turbulence in the Severe Windstorms

The one main area where the two- and three-dimensional simulation differ is in the modelling of turbulence. The observations show that surface wind speeds downstream of the mountain peak are characterized by a high degree of transients. Fig. 7 shows the observations for the 11 January 72 case. This figure shows a series of relatively low frequency spikes superimposed upon a much higher frequency. The three-dimensional simulations of Clark and Farley obtained a surface gustiness signature of

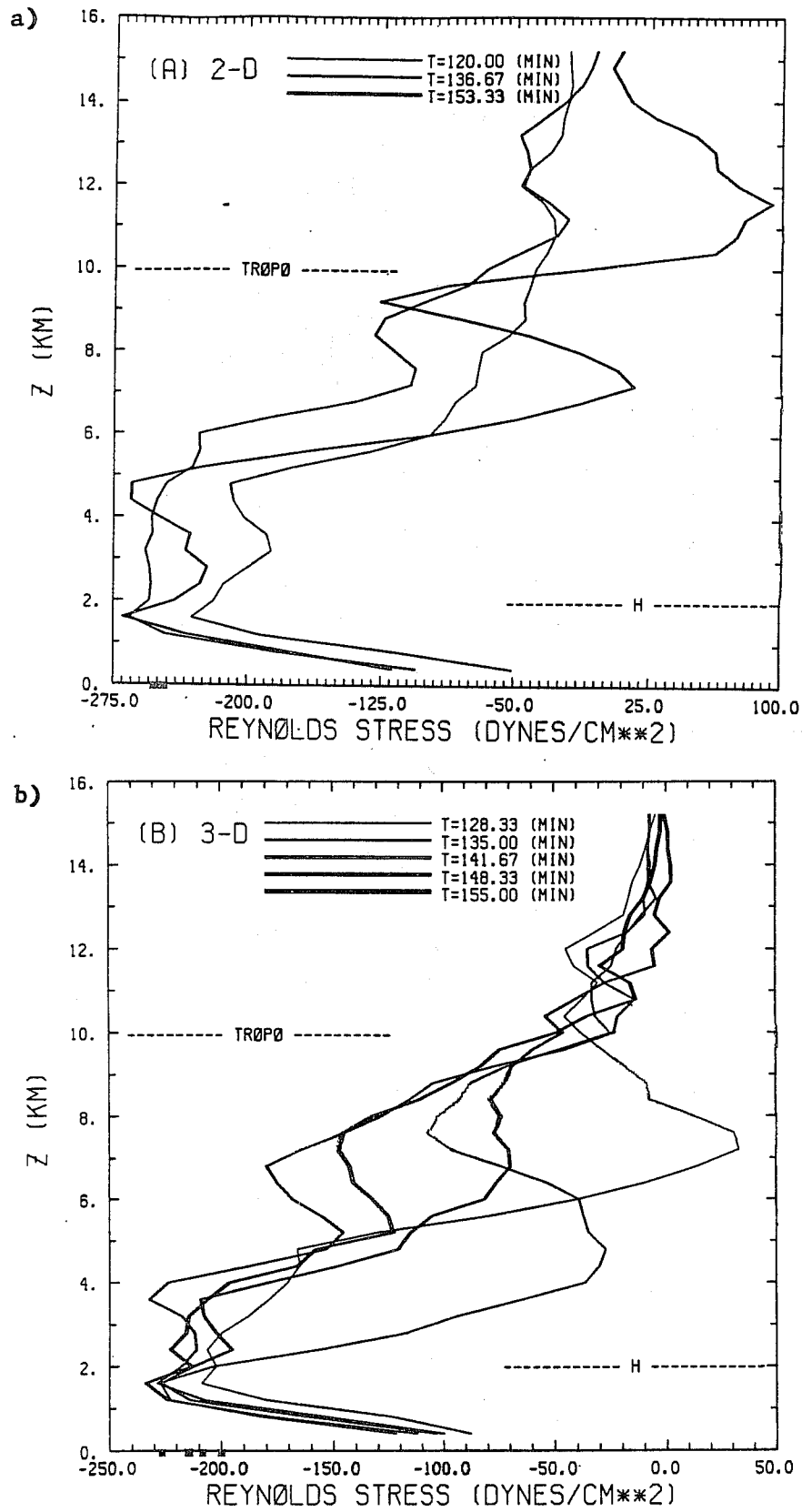

Fig. 4 Reynolds stress profiles from the simulations of Clark and Farley (1984) for the 11 January 1972 windstorm. Times are marked for each curve in min. a) two-dimensional calculation, b) three-dimensional calculation.

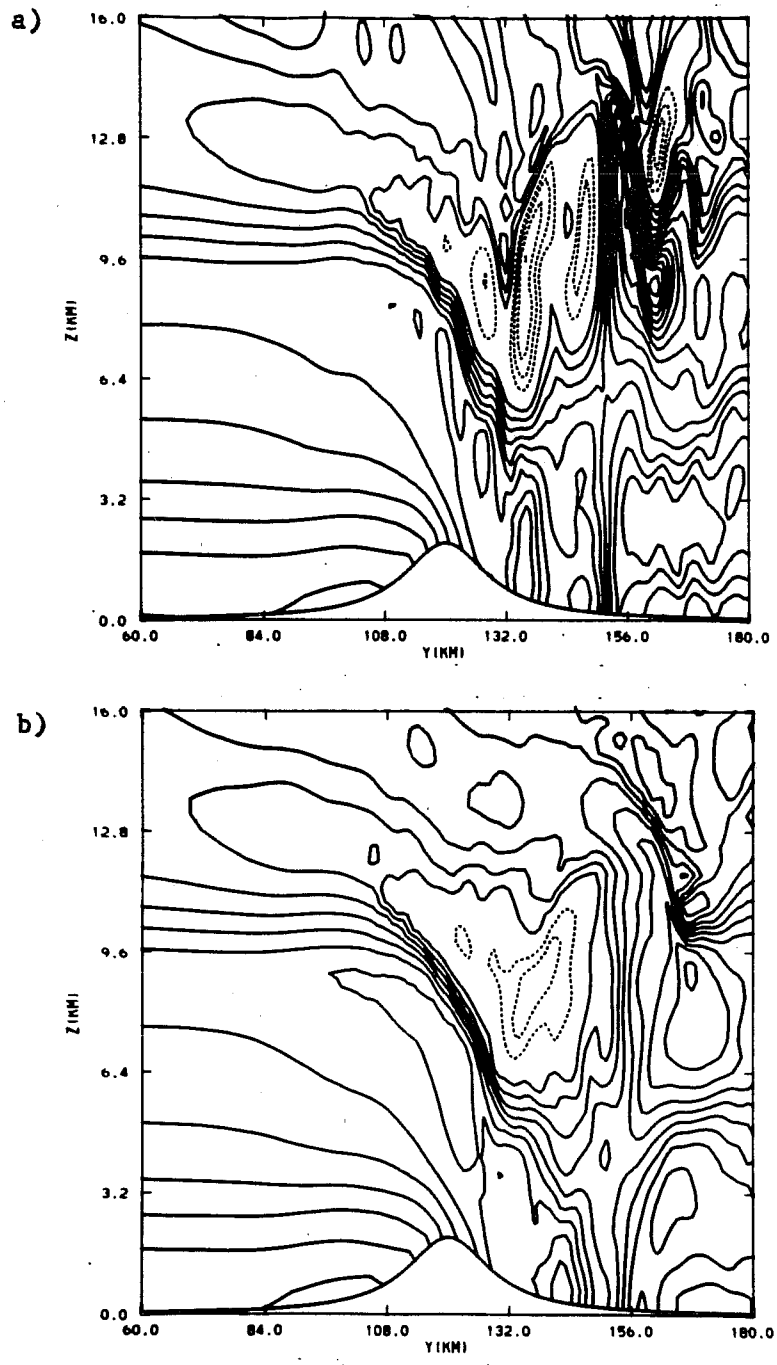

Fig. 5 U field comparison between two- and three-dimensional simulations. Contour interval is 8 m s^{-1}. Positive contours solid and negative contours dashed. No zero contour.

a) two-dimensional field at t = 153.33 min,
b) three-dimensional cross stream averaged field at t = 155 min.

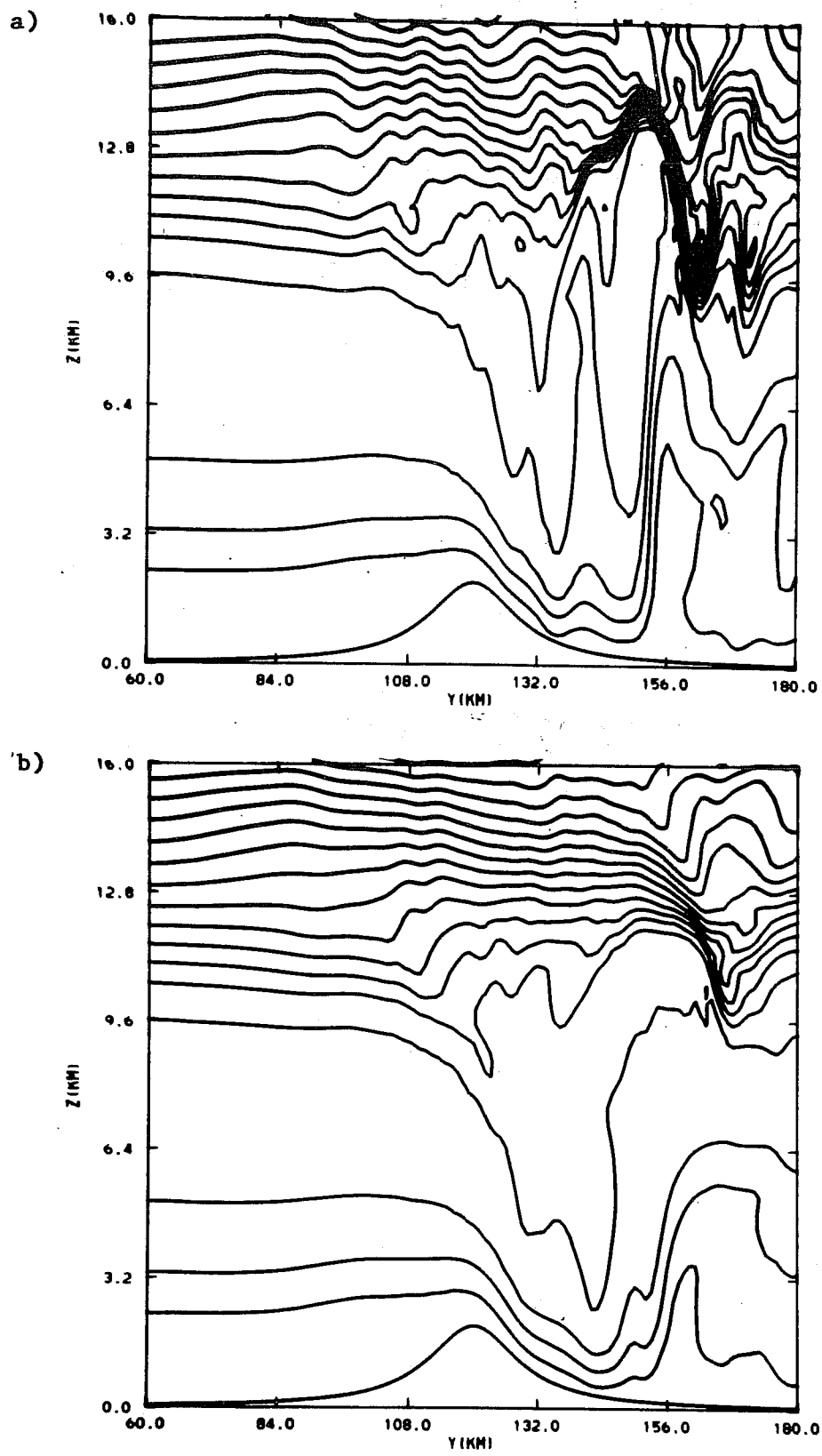

Fig. 6 Same as Fig. 5 except for θ field. Contour interval is 8 K.

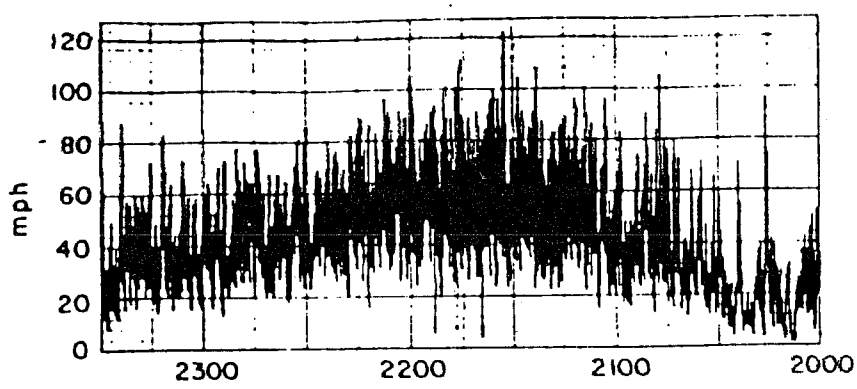

Fig. 7 Anemometer trace for 11 January 1972 windstorm in Boulder (after Klemp and Lilly, 1975).

the lower frequency character without the high frequency component. Peak gusts occurred on a frequency of about 10-15 min in their simulations, e.g. see their Fig. 14. The two-dimensional simulations, on the other hand, produce a steady surface wind speed.

Lilly (1978) estimated that shear production was the major source of turbulence production in the elevated regions and that surface roughness may have contributed to the lower level turbulence downstream of the mountain peak. Clark (1987) performed a turbulent kinetic energy budget analysis of the three-dimensional simulated case. He defined the turbulence as that portion of the flow which differed from the cross-stream averaged value. Fig. 8 shows the turbulent kinetic energy at $t = 140$ min. We see the turbulence occupying a large portion of the convectively unstable wave breaking region. There is also a region located downstream of the mountain extending from the ground up to about the 6 km level. The approximate location of Boulder is marked on the figure. The main source terms for the turbulence were found to be from the shear production terms. Fig. 9 shows the distribution of the shear production terms at $t = 155$ min. This time level shows most clearly how the source is confined to the leading lower edge of the inflowing air near the interface between the stable air and the convectively unstable region. Source/sink terms associated with the convection itself ($\overline{w'\theta'}$) were about an order of magnitude smaller than the shear terms. The final distribution of turbulence is established through shear production and advection much in the way as discussed by Lilly (1978).

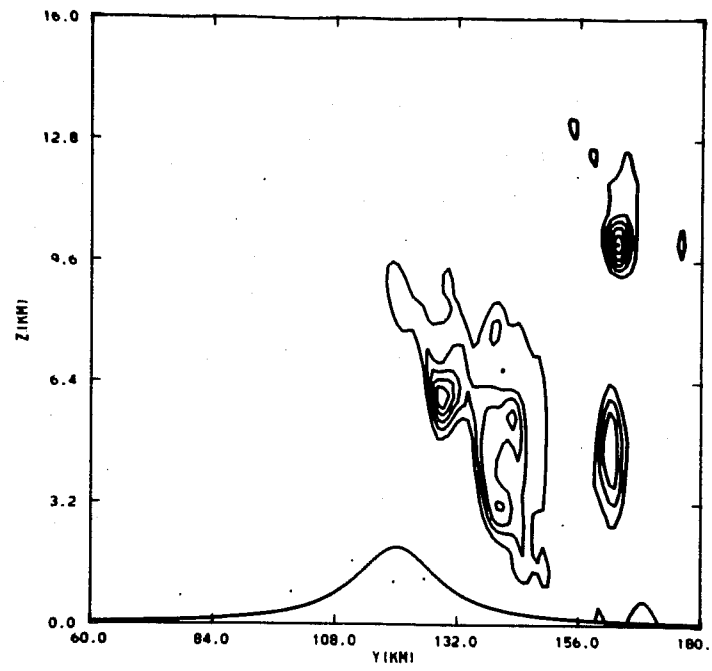

Fig. 8 Turbulent kinetic energy at t = 140 min for a three-dimensional simulation of the 11 January 1972 windstorm (after Clark, 1987). Contour interval is 16 Kg $m^{-1}s^{-2}$.

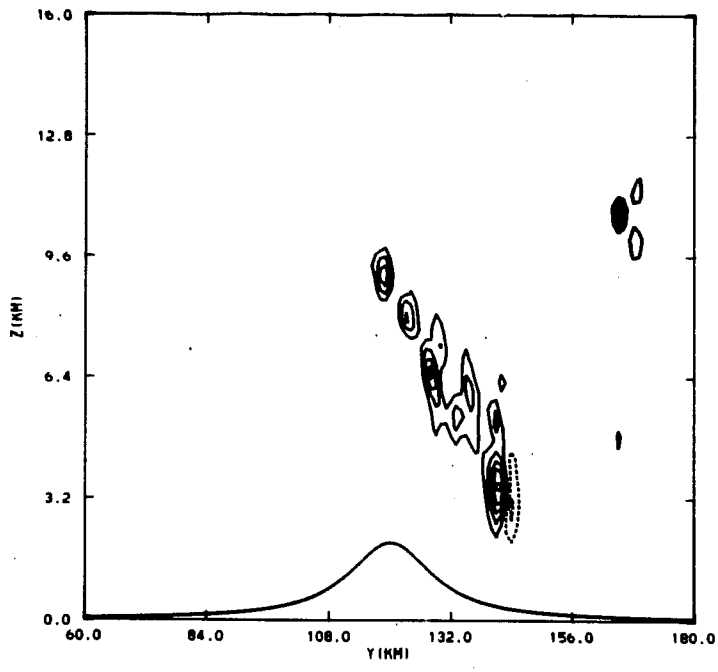

Fig. 9 Shear production terms of the turbulent kinetic energy budget. Contour interval is .25 Kg $m^{-1}s^{-3}$.

8. Conclusions

This paper has discussed certain technological aspects associated with the modelling of the wave dynamics of severe downslope windstorms. Those areas were highlighted where there appears to be some degree of misunderstanding in the literature as well as certain aspects where there is almost no discussion in the literature. There appears to be an under-emphasis in the literature discussing the degree to which initialization affects the results. The typically used initialization procedures were categorized with the idea in mind that this may aid in future assessments of this problem area. It was suggested in the text that the domain extent may have influenced the particular steady state wave drag response obtained by various simulations of the 11 January 1972 Boulder windstorm event. Resolution effects and equation filtering may have also influenced these predictions. It appears that there is a need for further systematic research on the response of air flowing over the major mountain barriers where upstream effects and initialization effects are more thoroughly considered.

A comparison between the two- and three-dimensional simulations of Clark and Farley (1984) and between the two-dimensional case of Peltier and Clark (1983) suggest that the Reynolds stresses for the severe windstorm event behave in a similar fashion to the supercritical homogeneous atmosphere case. A near equal rate of negative momentum deposition appears to occur between the mountain top and the nonlinear reflecting region set up by wave breaking. This result is quite different from that recently postulated by Lindzen (1981) and Holton (1982) based upon the earlier work of Hodges (1969) where they suggest the deposition is confined to the nonlinear wave breaking region itself. Furthermore, in the severe windstorm case there was shown to be a region of positive momentum deposition below mountain top or flow speed up in the lee of mountain. The differences in structure and amplitude of the stresses and mean fields between the two- and three-dimensional simulations appear to be minimal for the idealized severe windstorm simulations. There appears to be a need for much more extensive research in this area particularly for the three-dimensional case where more realistic turbulence and barrier effects can be simulated. The gustiness signatures obtained in the simulations of Clark and Farley were only partially successful in reproducing the observed gustiness. Resolution and/or idealizations of the surface forcing seen to be the most likely candidates for further investigations.

A significant emphasis was placed upon the advantages of using multi-domain nesting procedures with the non-hydrostatic models. It is believed that many of the current model restrictions can be greatly reduced through this procedure. A more in depth study of many of the previsouly modelled aspects of mountain drag should be possible using this approach.

References

Arakawa, A., 1966: Computational design for long term integration of the equations of motion: Two-dimensional incompressible flow. Part I. J. Comput. Phys., 1, 119-143.

Barcilon, A. and J. C. Jusem, 1979: On the two-dimensional, hydrostatic flow of a stream of moist air over a mountain ridge. Geophys. Astrophys. Fluid Dyn., 13, 125-140.

Batchelor, G. K., 1953: The condition for dynamical similarity of motions of a frictionless perfect-gas atmosphere. Quart. J. Roy. Meteor. Soc., 79, 224-235.

Beland, M. and T. Warn, 1975: The radiation condition for transient Rossby waves. J. Atmos. Sci., 32, 1873-1880.

Carpenter, K. M., 1979: An experimental forcast using a non-hydrostatic mesoscale model. Quart. J. Roy. Meteor. Soc., 105, 629-655.

Clark, T. L., 1987: Numerical Simulations of a severe downslope windstorm in three spatial dimensions: Eddy kinetic energy budget analysis. Aero Revue, in press.

Clark, T. L., 1986: Documentation of Clark's anelastic model: Version G2TC28. Report obtainable from author.

Clark, T. L., 1977: A small scale dynamic model using a terrain following coordinate transformation. J. Comp. Phys., 24, 186-215.

Clark, T. L. and R. D. Farley, 1984: Severe downslope windstorm calculations in two and three spatial dimensions using anelastic interactive grid nesting: A possible mechanism for gustiness. J. Amos. Sci., 41, 329-350.

Clark, T. L. and W. R. Peltier, 1984: Critical level reflection and the resonant growth of nonlinear mountain waves. J. Atmos. Sci., 41, 3122-3134.

Clark, T. L. and W. R. Peltier, 1977: On the evolution and stability of finite-amplitude mountain waves. J. Atmos. Sci., 34, 1715-1730.

Deaven, D. G., 1976: A solution for boundary problems in isentropic coordinate models. J. Atmos. Sci., 33, 1702-1713.

Durran, D. R. and J. B. Klemp, 1983: A compressible model for the simulation of moist mountain waves. Mon. Wea. Rev., 111, 2341-2361.

Dutton, J. A. and G. H. Fichtl, 1969: Approximate equations of motion for gases and liquids. J. Atmos. Sci., 26, 241-254.

Eliassen, A. and E. Palm, 1960: On the transfer of energy in stationary mountain waves. Geofys. Publ., 22, 1-23.

Gal-Chen, and R. C. J. Somerville, 1975: On the use of a co-ordinate transformation for the solution of the Navier-Stokes equations. J. Comput. Phys., 17, 209-228.

Hodges, R. R., Jr., 1969: Eddy diffusion coefficients due to instabilities in internal gravity waves, J. Geophys. Res., 74, 4087-4090.

Hoinka, K. P., 1985: A comparison of numerical simulations of hydrostatic flow over mountains with observations. Mon. Wea. Rev., 113, 719-735.

Holton, J. R., 1982: The role of gravity wave induced drag and diffusion in the momentum budget of the mesophere. J. Atmos. Sci., 39, 791-799.

Klemp, J. B. and D. R. Durran, 1983: An upper boundary condition permitting internal gravity wave radiation in numerical mesoscale models. Mon. Wea. Rev., 111, 430-444.

Klemp, J. B. and D. K. Lilly, 1978: Numerical simulation of hydrostatic mountain waves. J. Atmos. Sci., 35, 78-107.

Klemp, J. B. and D. K. Lilly, 1975: The dynamics of wave-induced downslope winds. J. Atmos. Sci., 32, 320-339.

Kurihara, Y., G. J. Tripoli, and M. A. Bender, 1979: Design of a moveable nested-mesh primitive equation model. Mon. Wea. Rev., 107, 239-249.

Kwizak, M. and A. J. Robert, 1971: A semi-implicit scheme for grid point atmospheric models of the primitive equations. Mon. Wea. Rev., 99, 32-36.

Lilly, D. K., 1978: A severe downslope windstorm and aircraft turbulence event induced by a mountain wave. J. Atmos. Sci., 35, 59-77.

Lilly, D. K. and J. Klemp, 1979: The effects of terrain shape on nonlinear hydrostatic mountain waves. J. Fluid Mech., 95, 241-261.

Lilly, D. K. and E. J. Zipser, 1972: The front range windstorm of 11 Jan 1972 -- a meteorological narrative. Weatherwise, 25, 56-63.

Lindzen, R. S., 1981: Turbulence and stress owing to gravity wave and tidal breakdown. J. Geoph. Res., 86, 9707-9714.

Mahrer, Y. and R. A. Pielke, 1977: A numerical study of the airflow over irregular terrain. Contrib. Atmos. Phys., 50, 98-113.

Marchuk, G. I., 1974: Numerical Methods In Weather Prediction. Academic Press, New York and London.

Mason, P. J. and R. I. Sykes, 1978: A simple Cartesian model of boundary layer flow over topography. J. Comput. Phys., 28, 198-210.

Miles, J. W. and H. E. Huppert, 1969: Lee waves in a stratified flow. Part 4. Perturbation approximations. J. Fluid Mech., 35, 497-525.

Ogura, Y. and N. A. Phillips, 1962: Scale analysis of deep and shallow convection in the atmosphere. J. Atmos. Sci., 19, 173-179.

Peltier, W. R. and T. L. Clark, 1979: The evolution and stability of finite amplitude mountain waves. Part II: Surface wave drag and severe downslope windstorms. J. Atmos. Sci., 36, 1498-1529.

Peltier, W. R. and T. L. Clark, 1983: Nonlinear mountain waves in two and three spatial dimensions. Quart. J. Roy. Meteor. Soc., 109, 527-548.

Pierrehumbert, R. T. and B. Wyman, 1985: Upstream effects of mesoscale mountains. J. Atmos. Sci.m 42, 977-1003.

Schuman, F. G., 1962: Numerical experiments with the primitive equations Proc. International Symposium on Numerical Weather Prediction, Tokyo, Meteor. Soc., Japan, 85-107.

Scorer, R. S., 1949: Theory of waves in the lee of mountains. Quart. J. Roy. Meteor. Soc., 75, 41-56.

Tapp, M. C. and P. W. White, 1976: A non-hydrostatic mesoscale model. Quart. J. Roy. Meteor. Soc., 102, 277-296.

Tripoli, G. J. and W. R. Cotton, 1982: The Colorado State University three-dimensional cloud/mesoscale model -- 1982. Part I: General theoretical framework and sensitivity experiments. J. Rech. Atmos., 16, 185-219.